Interaction between overlapping photo-ionized doubly excited resonances series for He atom

T. N. Chang[1], T. K. Fang[2], and X. Gao[3,*]

[1] Department of Physics, Univ. of Southern California, LA, CA 90089-0484, U.S.A.
[2] Department of Physics, Fu Jen Catholic University, Taipei, Taiwan, 242, ROC
[3] Beijing Computational Science Research Center, Beijing, 100084, China

Abstract

We present a detailed theoretical study on the photoionization from the bound excited ^1P state of He to continua dominated by multiple doubly excited resonance series embedded in multiple single-ionization channels between the $N = 2$ and $N = 3$ thresholds. In addition to identifying the individual resonance series, our investigation has also demonstrated unambiguously the level crossing between overlapping resonance series and how the closely spaced pairs of resonances migrate as energy increases.

PACS: 32.80.Fb; 32.80.Zb; 32.70.Jz; 32.80.Xx

I. INTRODUCTION

Rapid advances in the free-electron laser (FEL) [1] and the higher-order harmonic generation [2] during the past decade have made the coherent UV and XUV radiation readily available to study atomic processes in greater details that were unattainable previously. Among them are the characterizations of some of the most fundamental processes, which are difficult to analyze experimentally without the detailed theoretical understanding. One such example is the question on the direct versus sequential ionization when the photon energy is sufficient to ionize both electrons from the simplest two-electron atom [3, 4]. To characterize such process fully, it requires the detailed transition rates for a number of transitions, including those coupled with intermediate doubly excited resonant states in the continua, along various paths leading to the final continua (see, e.g., Fig. 1 of [4]). Below the double ionization threshold of the two-electron atom, the atomic spectra are dominated by a large number of *overlapping* doubly excited resonance series. The need for accurate transition rates for processes beyond the well understood ^1S to ^1P transitions from the ground state is clearly required.

The detailed atomic structure studies, both experimentally and theoretically, of the single photoionization of He were responsible for much of the current understanding of multi-electron interactions in atomic transitions [5-8]. With the high resolution experimental observations, the atomic transitions from the ^1S ($J = 0$) ground state of He to the ^1P ($J = 1$) final states (either to the bound excited states, the structure-less continua, or continua dominated by doubly excited resonances series) have been the testing ground for the atomic structure theories during the past few decades [9-11]. The pump-and-probe experiments, which are instrumental in the understanding of atomic structures for more active heavier atoms [12], are unfortunately limited for He atom due to the lack of shorter wavelength light source to elevate the atom to the bound excited states. As a result, the detailed studies of the atomic processes, other than the $^1S \rightarrow {}^1P$ transitions, are not broadly available for simple system such as He atom. Unlike the heavier atoms with their spectra mostly classified by the usual LS or jj coupling, the degenerate thresholds and the non-LS coupling characteristic makes the study of the electron-electron interaction in He particularly interesting. With the availability of the shorter wavelength light sources in UV and XUV region, it is now possible to carry out detailed experimental measurement for atomic transitions starting from states other than those with ^1S symmetry to final states with symmetry beyond ^1P. In addition, to characterize correctly the multi-photon processes, it is critical to compile the accurate theoretical estimates of transition rates beyond the basic $^1S \rightarrow {}^1P$ transitions as discussed above.

By analyzing theoretically the components of the S-matrix, interactions between doubly excited resonance series were studied earlier [10, 11] in details on the ^1P resonances series for transitions from the He ground state with focus on the complicated spectral region closed to the doubly ionization threshold where a large number of resonances are embedded in a large number of single-ionization channels in a very narrow spectral region. For example, there are nine doubly excited ^1P resonance series embedded in sixteen single-ionization channels between the $N = 4$ and $N = 5$ thresholds. To compare with the observed spectra, the reported theoretical spectra represent mostly the cross sections (i.e., the sum of convoluted partial cross sections into a number of single-ionization channels) against each of the ionization threshold. Since the weak doubly excited resonance series are likely to be *hidden* under the more prominent resonance series and may not be observed experimentally (see, e.g., two such examples in Figs. 4-5 and Figs. 7-8 in [13]), what we present in this paper is an alternative approach to identify and analyze in details those weak but strongly overlapping resonances decaying into multiple sinlge-ionization channels.

The main purpose of this paper is to present a theoretical analysis of a proto-type photoionization process from the bound excited $1s2p\ ^1P$ state of He to final continua between the $N = 2$ and $N = 3$ ionization thresholds. Our study is focused on three overlapping doubly excited ^1S resonance series embedded in three single-ionization channels and six overlapping doubly excited ^1D resonance series in four single-ionization channels. We have chosen this particular spectral region since the number of overlapping resonance series and the number of single-ionization channels are still limited for a detailed theoretical analysis. We will also demonstrate in details the level crossing between overlapping resonance series and how they migrate due to the interaction between series. Our discussions are based on the theoretical spectra derived from two distinct theoretical approaches, the B-spline-based K-matrix (BSK) method [14] and the eigenchannel R-matrix (ECR) method [15, 16]. One important advantage we enjoy in our present study is the ability to compare the theoretical results from these two different calculations. The overall agreement for an extended energy region between the calculated spectra from these two calculations suggests strongly their quantitative reliability. In addition, both calculations have also led to agreement between the length and velocity results to 1% or better.

We will review briefly the basics of the BSK and ECR approaches in Sec. II. In Sec. III, we present the detailed results and discussions of our calculated theoretical spectra. We will also illustrate how we are able to identify each of the doubly excited resonance through the energy variation of the sum of the eigen-phase shifts over all contributing

eigenchannels.

II. THEORETICAL APPROACHES

A. B-spline based K-matrix method

For multi-channel photoionization, Fang and Chang [14] have extended an earlier B-spline based configuration interaction method (BSCI) [7] for single ionization channel to a B-spline based K-matrix method (BSK) following the usual K-matrix approaches [6, 17]. An eigenchannel Γ at a total energy E is represented as a linear combination of individual open channel wavefunctions $|\Phi_{\gamma_o E}\rangle$, i.e., [14]

$$|\,\Gamma E\rangle = \sum_{\gamma_o} |\Phi_{\gamma_o E}\rangle\; U_{\gamma_o \Gamma}(E)\; cos\,\eta_\Gamma(E), \tag{1}$$

where $U_{\gamma_o\Gamma}(E)$ is an orthogonal transformation matrix and the eigenphase shift η_Γ represents the interactions between $|\Phi_{\gamma_o E}\rangle$. Similar to the *normal modes* of a complex system, the *eigenchannels* are intimately related to the dynamics of the atomic process, although they do not in general represent directly the individual atomic states.

The eigenstate $|\Gamma E\rangle$ satisfies the *orthonormality* relation

$$\langle \Gamma' E' \,|\Gamma E\,\rangle = \delta_{\Gamma'\,\Gamma}\,\delta\,(E' - E)\,. \tag{2}$$

The transformation matrix $U_{\gamma_o\Gamma}(E)$ and the eigenphase shift η_Γ are obtained by diagonalizing the *on the energy shell* K-matrix, i.e.,

$$\sum_{\gamma} \langle \gamma_o E \,|\, K(E)\,|\gamma E\,\rangle\, U_{\gamma\Gamma} = -\pi^{-1} \tan\eta_\Gamma\, U_{\gamma_o\Gamma} \tag{3}$$

where the K-matrix, expressed as a set of coupled integral equations, is given explicitly by Eq. (11) in [14]. Similar to the increase of the scattering phase shift by a value of π across a resonance embedded in a single continuum, the sum of the eigenphase shift over all eigenchannels, i.e.,

$$\eta_{tot} = \sum \eta_\gamma \tag{4}$$

also increases by a total of π as the energy increases across an isolated resonance. The width of a resonance can be derived from the energy variation of η_{tot}. We should note that such procedure is well established in atomic structure calculation (e.g., see the similar application in [11]).

As detailed in [14], the total photoionization cross section σ_{tot} is given by the sum of the partial cross sections over all open channels, i.e.,

$$\sigma_{tot} = \sum_{\gamma} \sigma_{\gamma} \,. \tag{5}$$

The partial cross section in unit of a_0^2 for each open channel γ is given by

$$\sigma_{\gamma} = 4\pi^2 \alpha \, f_{\gamma I} \tag{6}$$

where the effective oscillator strengths $f_{\gamma I}$ from an initial state I, corresponding to length and velocity approximations are given by Eqs. (22) and (23) in [14], respectively.

B. Eigenchannel R-matrix method

Over the years, the R-matrix approach has been successfully developed as an *ab-initio* method for treating a variety of dynamic processes in atomic physics [18-22]. The basic idea of the R-matrix theory is to partition configuration space into sub-regions, each with different physical property that dictates the atomic processes. A different and appropriate representation of the wave function is adopted in each region. These wave functions are connected by the R-matrix defined on their common boundary, i.e., at $r = r_o$. Recently, Gao and Li have extended both the non-relativistic and relativistic versions of the eigenchannel R-matrix method, referred to as R-eigen and R-R-eigen, respectively [15, 16], from the earlier Breit-Pauli [19] and Dirac R-matrix codes [20]. With the ECR method, we are able to obtain the scattering matrices corresponding to the physical parameters associated with the multichannel quantum defect theory (MQDT) [22-25] for both the discrete and continuous energy regions of interest. Various physical quantities can then be derived from a straightforward application of the MQDT procedure.

Specifically, the logarithmic derivative boundary matrix $R(E)$ is obtained by first solving the $(N+1)$-electron problem variationally within the reaction zone, i.e., the R-matrix box. For the R-eigen code, the one-particle Hamiltonian is non-relativistic with or without the Breit-Pauli terms, whereas for the R-R-eigen code, the Dirac-Coulomb Hamiltonian is employed. The reaction matrix $K(E)$ is calculated with the standing-wave expressions on the boundary of the reaction zone, i.e., at $r_o = r_{N+1}$

$$\Psi_i(E) = \Phi_i f_i(r_o, E) + \sum_{j=1}^{n_p} \Phi_j g_j(r_o, E) K_{ij} + \sum_{j=n_p+1} \Phi_j \Theta_j(r_o, E), \quad i \le n_p \tag{7}$$

where i and j are the channel indices. The wave function Φ_i consists of the N-electron target-state wave function combined with the angular and spin parts of the wave function of the $(N+1)^{th}$ electron in the i^{th} channel. In the energy region of interest, only finite number of channels contribute directly to the observed spectral structures. They are known as the physical channels ($i \leq n_p$). For the i^{th} physical (i.e. ionization) channel, the regular and irregular Coulomb wave functions, $f_i(r,E)$ and $g_i(r,E)$, modified by the appropriate long-range polarization interactions, cover the entire set of one-electron orbitals, with both negative and positive energy [8]. With Eq. (7), in what is known as the "semiscattering" physical picture, we are able to extend the scattering matrices normally defined only in the positive energy regions to the whole energy regions. For the other contributing channels ($j > n_p$) at a total energy E with the core state Φ_j at higher energy, the corresponding radial wave functions Θ_j of the $(N+1)^{th}$ electron should have fairly negative orbital energies and exponentially decaying radial wave function with negligible magnitude at $r_{N+1} = r_o$. All such channels with $j > n_p$ are called the computational channels. They are included in our calculation to assure that the electron correlations are taken into account adequately.

In the eigenchannel representation, following the details outlined elsewhere [8,21-24] and similar to the K-matrix in Eq. (3) shown earlier for the BSK approach, the short-range reaction matrix with total angular momentum J is expressed in terms of the smoothly varying eigenchannel parameters in energy, i.e., eigen-quantum defect ν_α and the $n_p \times n_p$ orthogonal transformation matrix $U_{j\alpha}$ by

$$K^J_{ij} = \sum_\alpha U_{i\alpha} \tan(\pi\nu_\alpha) U_{j\alpha}. \tag{8}$$

The corresponding eigenchannel wavefunction ψ_α is normalized per unit energy and represents the detailed dynamic characters of an excited electron and its interactions with the ionic core within the reaction zone. The state functions are then expressed as the linear combination of eigenchannel wavefunctions, i.e.,

$$\Psi^J(E) = \sum_\alpha A_\alpha \, \psi_\alpha(E) \tag{9}$$

where A_α is the mixing coefficient and determined by the asymptotic boundary conditions [24]. The transition rate, or, the oscillator strength $f(E)$ is given by

$$f(E) = \frac{2(E-E_o)}{N^2} \mid \sum_\alpha D_\alpha \cdot A_\alpha \mid^{\,2} \tag{10}$$

where N is the normalization factor and $D_\alpha = < \psi_\alpha | D | \Psi_o >$ is the dipole matrix element for transition to the specific eigenchannel ψ_α from the initial state Ψ_o with energy E_o.

III. RESULTS AND DISCUSSIONS

For the single photoionization with photon energy between the $N = 2$ and $N = 3$ thresholds from the bound excited ^1P state of He, there are three doubly excited resonance series for the $^1P \rightarrow {}^1S$ transition leading into three ionization channels (i.e., $1s\epsilon s$, $2s\epsilon s$, and $2p\epsilon p$) and six doubly excited resonance series for the $^1P \rightarrow {}^1D$ transition leading into four ionization channels (i.e., $1s\epsilon d$, $2s\epsilon d$, $2p\epsilon p$, and $2p\epsilon f$). Earlier study on the ^1S and ^1D doubly excited resonances of He above the $N = 2$ threshold depends primarily on the complex rotation method [26-29], which is capable of estimating the energy and width of the doubly excited resonance. No attempt, however, was made to investigate the detailed spectra for the atomic transitions such as the ones presented in this paper.

Figure 1 presents the theoretical photoionization spectra from the bound excited $1s2p\ ^1P$ state to the ^1D continua. The top plot represents the spectrum calculated with the BSK approach and the bottom one with the ECR approach. It is clear that the agreement between the two calculations is excellent. In addition, the length and velocity results are nearly identical in both calculations. Only four resonance series are labeled in Fig. 1. To facilitate our discussion below, we have labeled the four overlapping resonance series as $A_n((2,0)^+_n)$, $B_n((0,2)^+_n)$, $C_n((0,0)^+_n)$, and $D_n((1,1)^-_n)$ under the classification scheme in terms of a set of correlation quantum numbers K, T, and A in the form of $(K,T)^A_n$ [30]). A more detailed spectrum on the higher energy side of Fig. 1 up to 3.7785 Ry is presented in Fig. 2, together with the energy variation of the η_{tot} obtained from the BSK calculation. Two additional resonance series $E_n((-1,1)^0_n)$ and $F_n((-2,0)^0_n)$ are identified in the top plot of Fig. 2. Each of the doubly excited resonance could easily be identified by the increase of π in η_{tot}. Interestingly, Fig. 1 shows that the two resonances A_4 and D_4 are fairly closely located whereas there is substantial separation between C_3 and A_4. However, at higher energy, as shown in Fig. 2, the resonance series D_n clearly moves away from the series A_n. On the other hand, the energy separation between the pairs of adjacent resonances A_{n+1} and C_n are getting progressively smaller as n increases. It is only from the increases of 2π in η_{tot} near 3.763 Ry and 3.775 Ry that we are able to confirm the presence of two pairs of closely spaced overlapping resonances (C_5, A_6) and (A_7, C_6), respectively.

The question one should then ask is if the resonance C_n will move to the higher energy side of the resonance A_{n+1}, i.e., if there is a level crossing between these two resonance series. If, indeed, the level crossing occurs, how do these two overlapping resonance series migrate as energy increases? To answer these two questions, we first

examine the partial cross sections into the four open channels (i.e., $1s\epsilon d$, $2s\epsilon d$, $2p\epsilon p$, and $2p\epsilon f$) for four pairs of resonances (A_5, C_4), (A_6, C_5), (C_6, A_7), and (C_7, A_8) shown in Fig. 3. Clearly, the partial cross sections into the $1s\epsilon d$ (mid-dash curve) channel is substantially smaller than the ones into the $2s\epsilon d$ (solid curve), the $2p\epsilon p$ (short dash curve), and the $2p\epsilon f$ (long dash curve) channels. The overall narrower resonance-like structure of the partial cross sections into the $2p\epsilon f$ ionization channel (long dash curve) remains essentially the same, except for the minor broader shoulder for the (A_5, C_4) pair near 3.7407 Ry on the higher energy side of the higher peak near 3.7384 Ry. The broader resonance-like structure of the partial cross sections into the $2p\epsilon p$ ionization channel also retains its basic shape, except for the smaller peak near 3.7381 Ry on the lower energy side of the higher peak near 3.7405 Ry for the (A_5, C_4) pair. The structures of the less prominent partial cross sections into the $2s\epsilon d$ ionization channel (solid curve), on the other hand, varies substantially from one pair of the resonances to the others. Our calculation shows a slow migration from a two peaks structure with almost same peak height for the (A_5, C_4) pair, to a structure of higher peak on the higher energy side for the (A_6, C_5) pair, and eventually to the ones of higher peak on the lower energy side for the (C_6, A_7) and (C_7, A_8) pairs. Together with the other switch-over of partial cross section peaks between the narrower peak into the $2p\epsilon f$ ionization channel (long dash curve) and the broader peak into the $2p\epsilon p$ ionization channel (short dash curve) as the pair of adjacent resonances migrates along the resonance series, it is clear that the level crossing indeed occurs between the two overlapping resonance series A_n and C_n. We should point out that the earlier theoretical work for the ^1P resonances for He has also analyzed the migration of the closely overlapping resonances (see, e.g., Figs 3 and 4 in [11]). However, the specific resonances were only expressed in terms of their sequential numerical designation, instead of their corresponding K, T, and A quantum numbers like those shown in Fig. 3.

By taking advantage of the ability of the B-spline based approaches [7, 14] to examine in details the state function of each resonance, as it migrates along the resonance series, we are able to check the detailed characteristics of each individual resonance to assure its proper assignment in terms of the probability densities corresponding to the contributing electronic configurations. In the present study, we first examine the bound component of the state functions of the resonances in a BSCI calculation by excluding all open-channel configurations. The top plot of Fig. 4 represents the variation of the effective quantum defect $\delta_{eff} = i - n^*$ for the A_i and C_i series, where n^* is the effective quantum number against the $N = 3$ threshold. The bottom plot represents the effective quantum numbers derived from the full BSK calculation with the energies of each resonance determined from the variation of η_{tot} shown in Fig. 2. As discussed above, the assignment of each individual resonance is confirmed from the detailed characteristics of its corresponding

state function. It is clear that the level crossing between these two overlapping resonance series indeed occurs as expected from the earlier discussion. The energies and widths of a few lowest ^1D resonances between $N = 2$ and $N = 3$ thresholds were calculated earlier with the complex rotation method with no specific assignment to their respective resonance series [26]. Numerically, those data are in good agreement with the results from the present study.

Figure 5 presents the theoretical photoionization spectra for the $1s2p\ ^1P$ to ^1S continua. Similar to the photoionization spectra into the ^1D continua shown in Fig. 1, the top plot represents the spectrum calculated with the BSK approach and the bottom one with the ECR approach. The agreement between the two calculations is again excellent and the length and velocity results are nearly identical in both calculations. Again, for simplicity, we have labeled the three overlapping resonance series as A_n, B_n, and C_n (which represent, respectively, the $(2,0)^+_n$, $(0,0)^+_n$, and $(-2,0)^+_n$ series). A more detailed spectrum on the higher energy side of Fig. 5 is presented in Fig. 6, together with the energy variation of the η_{tot} obtained from the BSK calculation. Similar to our early discussion, each of the doubly excited resonance could easily be identified by the increase of π in η_{tot}. Our calculated spectrum shows that the energy separation between the pairs of adjacent resonances A_{n+2} and C_n gets progressively smaller as n increases. In fact, the increase of 2π in η_{tot} near 3.773 Ry suggests the presence of two closely spaced overlapping resonances C_5 and A_7, which would be very difficult to identify from experimental spectra even at very high energy resolution. All the resonances in each of the resonance series discussed below are identified in terms of the energy variation of η_{tot}.

We now turn to the question once again on the level crossing, if it indeed occurs, between the A_n and C_n resonance series. Similar to Fig. 3, Fig. 7 presents the partial cross sections into three outgoing ionization channels, i.e., $1s\epsilon s, 2s\epsilon p$, and $2p\epsilon p$. The four plots shown in Fig. 7 represent the partial cross sections at energies near the vicinity of four pairs of resonances, i.e., i) $C_5((-2,0)^+_5)$ and $A_7((2,0)^+_7)$, ii) $C_6((-2,0)^+_6)$ and $A_8((2,0)^+_8)$, iii) $A_9((2,0)^+_9)$, and $C_7((-2,0)^+_7)$, and iv) $A_{10}((2,0)^+_{10})$, and $C_8((-2,0)^+_8)$, respectively. We note first that the partial cross sections into the $1s\epsilon s$ (short dash curve) channel is substantially smaller than the ones into the $2s\epsilon s$ (solid curve) and $2p\epsilon p$ (long dash curve) channels.

The top left plot of Fig. 7 shows i) one group of distinct peaks in the partial cross sections into three ionization channels near 3.77312 Ry and ii) a broader but less prominent one near 3.77342 Ry. They correspond to the pair of resonances C_5 on the lower energy side and A_7 on the higher energy side shown in the top plot of Fig. 6 slightly

below 3.774 Ry. The assignment to C_5 and A_7 of these two resonances is also supported by their contributing electronic configurations based on a careful examination of the detailed characteristics of the state functions. The bottom left and top right plot of Fig. 7 represent the partial cross sections leading into three continua correspond to, respectively, the pair of resonances C_6 and A_8 near 3.78136 Ry and A_9 and C_7 near 3.78662 Ry. The presence of the two distinct groups of peaks in partial cross sections is no longer evident and the *overlap* of the two resonances is nearly *complete*. A closer look at the variation of η_{tot} for both pairs of resonances yields an energy separation of about 10^{-4} Ry between the two neighboring resonances. Unlike the pairs of neighboring ^1D resonances A_{n+1} and C_n, which retain their basic characteristics in terms of their contributing electronic configurations below and above the level crossing discussed earlier, these two pairs of neighboring resonances show a nearly complete mixing of the basic characteristics of the two overlapping resonance series A_{n+2} and C_n. The bottom right plot of Fig. 7 represents the partial cross sections for the pair of resonances A_{10} and C_8 between 3.79006 Ry and 3.79024 Ry. The basic characteristic of the strong resonance-like peaks in partial cross section near 3.79019 Ry show little difference from the corresponding ones in three previous plots and may be nominally assigned as the C_8, or, $(-2,0)_8^+$ resonance. A closer inspection of the calculated spectrum reveals the presence of a shoulder in the partial cross sections on the lower energy side of the strong peak into the $1s\epsilon s$ continuum and a broader and much less prominent one into $2p\epsilon p$ continuum near 3.79013 Ry, which could be attributed to the A_{10} resonance. The assignment of C_8 and A_{10} for this pair of resonances is also confirmed by the detailed characteristics of their respective state functions. As a result, we are in the position to conclude the level crossing of these two overlapping ^1S resonance series. Our conclusion is consistent with the earlier theoretical estimate of the resonance energies from the complex rotation calculation, although no discussion on the level crossing was presented (see, Table 3 of [28]). It is also supported by the substantial variation of the expectation values of the imaginary part of the interelectronic angle along the resonance series based on a subsequent complex rotation calculation (see, Fig. 2 of [29]).

Finally, in Table I, we present a more critical comparison of the theoretical data between our results and the ones from the earlier complex rotation calculations in terms of the energy separations between the adjacent resonances for each of the ^1S resonance series. The agreement is excellent at 1 meV or better, which is comparable to the best energy resolution of the current synchrotron radiation light source with photon energies near 50 eV. We should also note that the resonance widths derived from the present calculations are also in good agreement with those from the complex rotation calculations [26-28].

IV. CONCLUSIONS

We would like to first comment on one of the key advantages of applying jointly in the present study two different approaches, i.e., the BSK and the ECR approaches. For the resonances of lower n, both BSK and ECR methods are capable of generating highly accurate atomic spectra as shown earlier since both approaches take into account fully the short-range interactions. The long-range polarizations, which may not contribute much to the atomic processes for the resonances with lower n, could affect significantly the resonances of higher n and clearly need to be included in any theoretical calculation that cover an extended spectral region. The BSK method, with its atomic orbitals confined in a sphere with an arbitrarily large radius R, is capable of including the long-range interactions even for resonances with high n. It, however, requires substantially more computational efforts involving the diagonalization of non-sparse matrix of the size even greater than the 15,000 or larger in the present study for each R. The ECR approach, with its ability to calculate the smoothly varying eigenchannel physical parameters for subsequent application of MQDT, is capable of extending directly the accurate atomic data from resonances with lower n to those with higher n, where the accuracy of high precision theoretical and/or observed atom data are often lacking. Its ability to generate highly accurate atomic data, of course, depends critically on the proper match of the $(N+1)$-electron wavefunction inside the reaction zone at a relatively small $r = r_o$ with the outside wavefunctions corresponding to the physical channels in the form of Eq. (7), if the long-range polarization effects could be properly accounted for. The excellent agreement between the theoretical spectra from BSK and ECR methods suggests that the atomic data generated from BSK method for resonances of intermediate n with long range polarizations adequately included could be applied to calibrate the proper match of the inside and outside wavefunctions at a relatively modest r_o for the ECR calculation. It, in turn, could lead to accurate atomic data for resonances with much higher n by applying the well established MQDT procedure.

In summary, we have presented in this paper detailed theoretical spectra for the continua dominated by multiple doubly excited resonance series embedded in multiple single-ionization channels. We should also point out that with the state functions generated explicitly in the present study, we are able to examine critically the migration of individual resonance along the resonance series and identify unambiguously the individual resonance, even for those closely spaced pairs of resonances near the level crossing between two overlapping resonance series. At the same time, we have made a critical step in the development of the necessary theoretical tools for a more detailed study of the multi-photon processes since the doubly excited ^1S and ^1D resonances studied in this

work are the same intermediate states that are expected to dominate the spectra of the two photon processes starting from the $1s^2$ ground state. The relevant dipole transition matrices such as the smooth varying D_α and the mixing coefficients A_α, corresponding to each eigenchannel associated with both the intermediate and final states of the multi-photon process, could be obtained from calculations such as the ones presented in this paper.

ACKNOWLEDGMENTS

This work was supported by the National Science Council in Taiwan under Grants No. NSC 100-2112-M-030-001 and NSC 103-2119-M-07-003, the National Science Foundation of China under Grant Nos. 11274035 and 11328401, the National Basic Research Program of China under the Grant Nos. 2010CB922900 and 2011CB921501, and the National High-Tech ICF Committee in China. One of us (TNC) would like to thank the partial support of the Norris Research Fund at USC.

References

[1] W. Ackermann *et al*, Nature Photonics **1**, 336 (2007); B. McNeil, Nature Photonics **3**, 375 (2009); S. Jamison, Nature Photonics **4**, 589 (6, 2010); P. Emma *et al*, Nature Photonics **4**, 641 (2010); I.Grguras at al, Nature Photonics **6**, 852 (2012); and references therein.

[2] N. A. Papadogiannis, L. A. A. Nikolopoulos, D. Charalambidis, G. D. Tsakiris, P. Tzallas, and K. Witte, Phys. Rev. Lett. **90**, 133902 (2003); Y. Nabekawa, H. Hasegawa, E. J. Takahashi, and K. Midorikawa, Phys. Rev. Lett. **94**, 043001 (2005); E. J. Takahashi, T. Kanai, K. L. Ishikawa, Y. Nabekawa, and K. Midorikawa, Phys. Rev. Lett. **99**, 053904 (2007); E. J. Takahashi, T. Kanai, K. L. Ishikawa, Y. Nabekawa, and K. Midorikawa, Phys. Rev. Lett. **101**, 253901 (2008); and references therein.

[3] A. Emmanouilidou1, V. Hakobyan, and P. Lambropoulos, J. Phys. B **46**, 111001 (2013); P. Lambropoulos, G. M. Nikolopoulos, and K. G. Papamihail, Phys. Rev. A **83**, 021407R (2011); P. Antoine, E. Foumouo, B. Piraux, T. Shimizu, H. Hasegawa, Y. Nabekawa, and K. Midorikawa, Phys. Rev. A **78**, 023415 (2008); R. Shakeshaft,

Phys. Rev. A **76**, 063405 (2007); B. Piraux, J. Bauer, S. Laulan, and H. Bachau, H Eur. Phys. J. D **26**, 7 (2003); M. S. Pindzola and F. Robicheaux, J. Phys. B. **31**, L823 (1998); and references therein.

[4] T. Nakajima and L. A. A. Nikolopoulos, Phys. Rev. A **66**, 041402(R) (2002).

[5] R. P. Madden and K. Codling, Phys. Rev. Lett. **10**, 516 (1963); J. W. Cooper, U. Fano, and F. Prats, Phys. Rev. Lett. **10**, 518 (1963).

[6] A. F. Starace, in *Handbuch der Physik, Theory of Atomic Photoionization* Ed. W. Mehlhorn, *Springer-Verlag, Berlin, 1982* pp. 1-121.

[7] T. N. Chang, in *Many-body Theory of Atomic Structure and Photoionization*, Ed. T. N. Chang *World Scientific, Singapore, 1993*, pp. 213-247.

[8] M. Aymar, C. H. Greene, and E. Lue-Koenig, Rev. Mod. Phys. **68**, 1015 (1996).

[9] K. Schulz, G. Kaindl, M. Domke, J. D. Bozek, A. Heimann, A. S. Schlachter, and J. M. Rost, Phys. Rev. Lett. **77**, 3086 (1996).

[10] I. Shimamura, J. Phys. B **44**, 201002 (2011); A. Menzel, S. P. Frigo, S. B. Whitfield, C. D. Candwell, M. O. Krause, T. J. Tang and I. Shimamura, Phys. Rev. Lett. **75**, 1479 (1995).

[11] K. Aiba, A. Igarashi, and I. Shimamura, J. Phys. B **40**, F9 (2007).

[12] F. J. Wuilleumier and M. Meyer, J. Phys. B **39**, R425 (2006).

[13] H. S. Fung, H. H. Wu, T. S. Yih, T. K. Fang, and T. N. Chang, Phys. Rev. A **64**, 052716 (2001).

[14] T. K. Fang and T. N. Chang, Phys. Rev. A **61**, 062704 (2000).

[15] X. Gao and J.-M. Li, Chin Phys. Lett. **29**, 033101 (2012).

[16] X. Gao and J.-M. Li, Phys. Rev. A **89**, 022710 (2014).

[17] V. Carravetta, P. Spizzo, R. Moccia, in *Many-body Theory of Atomic Structure and Photoionization*, Ed. T. N. Chang *World Scientific, Singapore, 1993*, pp. 175-212.

[18] P. G. Burke, *R-Matrix Theory of Atomic Collisions: Application to Atomic, Molecular and Optical Processes*, (Springer, Heidelberg, 2011).

[19] P. G. Burke and W. D. Robb, Adv. At. Mol. Phys. **11**, 143 (1975); K. A. Berrington, W. B. Eissner and P. H. Norrington, Comput. Phys. Commun. **92**, 290 (1995); M. J. Seaton, J. Phys. B **18**, 2111 (1985); K. A. Berrington *et al* J. Phys. B **20**, 6379 (1987).

[20] J. J. Chang, J. Phys. B **10**, 3335 (1975); P. H. Norrington and I. P. Grant, J. Phys. B **20**, 4869 (1987); S. Ait-Tahar, I. P. Grant and P. H. Norrington, Phys. Rev. A**54**, 3984 (1996).

[21] J. M. Li, Vo Ky Lan, Y. Z. Qu, J. Yan and P. H. Zhang, Phys. Rev. A**55**, 3239 (1997); X. Y. Han and J. M. Li, Phys. Rev. A **74**, 062711 (2006).

[22] U. Fano and J. M. Lee, Phys. Rev. Lett. **31**, 1573 (1973); C. M. Lee, Phys. Rev. A**10**, 584 (1974).

[23] W. Huang, Y. Zho, X. M. Tong, and J. M. Li, Phys. Rev. A**52**, 2770 (1995).

[24] C. M. Lee and K. T. Lu, Phys. Rev. A**8**, 1241 (1973).

[25] M. J. Seaton, Rep. Prog. Phys. **46**, 167 (1983).

[26] Y. K. Ho and J. Callaway, J. Phys. B **18**, 3481 (1985); Y. K. Ho and A. K. Bhatia, Phys. Rev. A**44**, 2895 (1991).

[27] Y. K. Ho, Phys. Rev. A**34**, 4402 (1986).

[28] A. Bürgers, D. Wintgen, and J-M Rost, J. Phys. B **28**, 3163 (1995).

[29] A. Bürgers, N. Brandefelt, and E. Lindroth, J. Phys. B **31**, 3181 (1998).

[30] C. D. Lin, Phys. Rev. Lett. **51**, 1348 (1983).

Table I. The energy separation ΔE (in Ry) between adjacent resonances for three ^1S resonance series.

n	Present	Ref. [29]	Ref. [27]
	$\Delta\ E\ (E_{A_{n+1}} - E_{A_n})$		
3	0.1448	0.1449	0.1449
4	0.0503	0.0502	0.0503
5	0.0241	0.0243	
6	0.0135	0.0134	
7	0.00807	0.00805	
8	0.00514	0.00521	
9	0.00357	0.00355	
	$\Delta\ E\ (E_{B_{n+1}} - E_{B_n})$		
3	0.1085	0.1081	0.1081
4	0.0335	0.0335	0.0333
5	0.0162	0.0162	
6	0.00925	0.00925	
7	0.00578	0.00579	
8	0.00388	0.00388	
	$\Delta\ E\ (E_{C_{n+1}} - E_{C_n})$		
3	0.0257	0.0261	
4	0.0139	0.0140	
5	0.00821	0.00827	
6	0.00532	0.00528	
7	0.00356	0.00358	

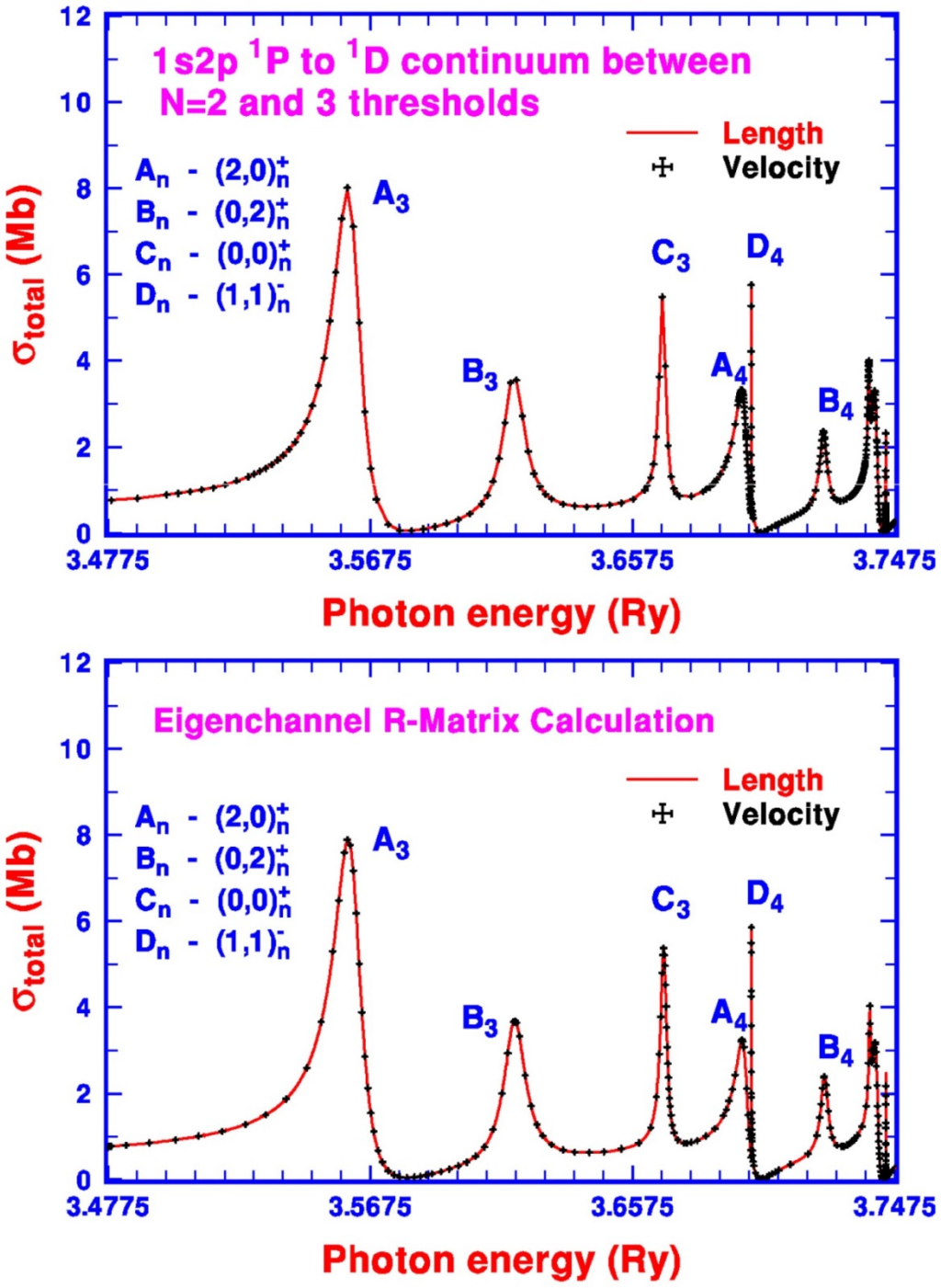

Fig. 1. (Color online) The theoretical photoionization spectra of He atom from the 1s2p ^{1}P bound excited state to the ^{1}D continua between N=2 and N=3 thresholds calculated with BSK method (top plot) and ECR method (bottom plot).

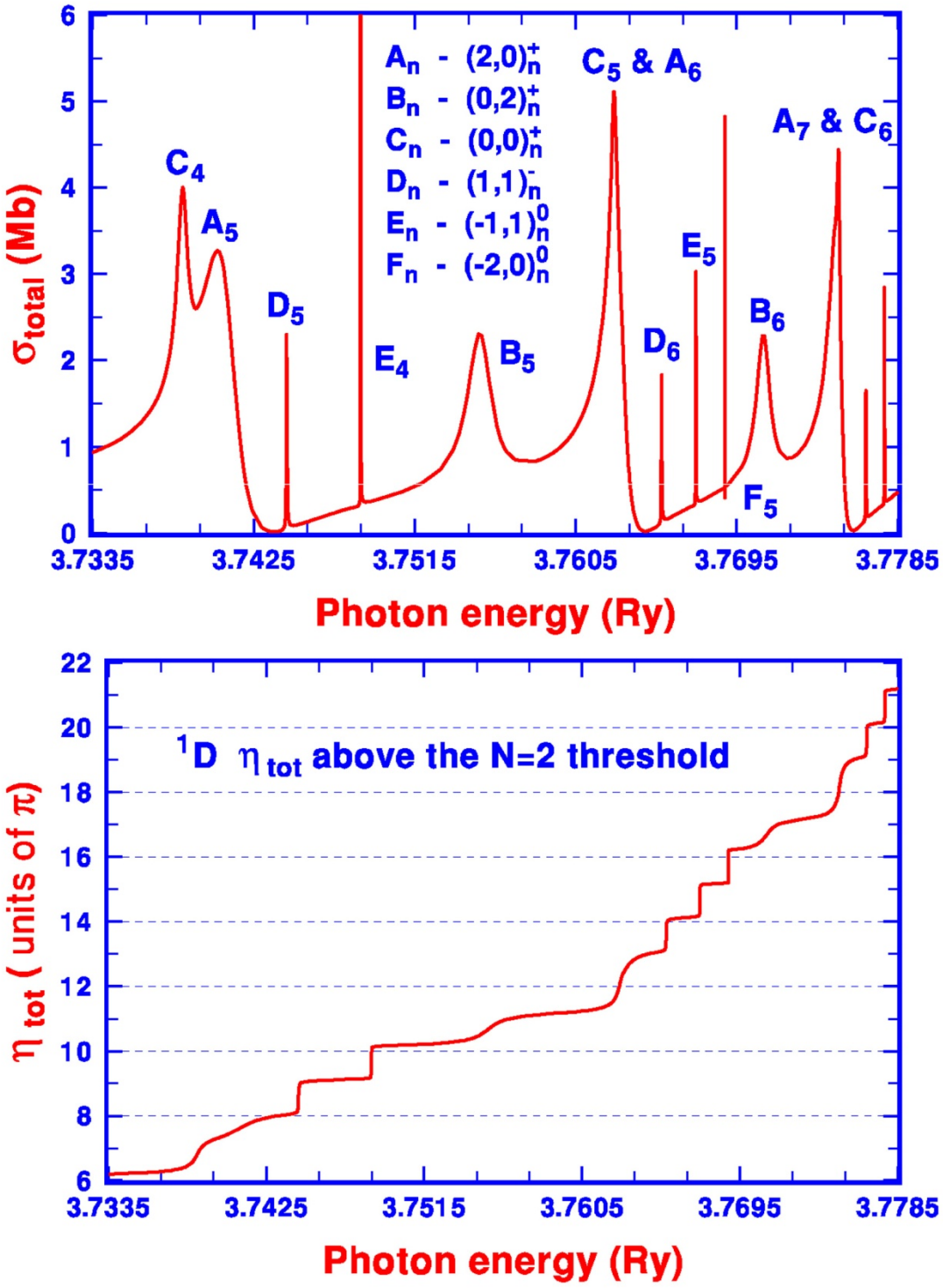

Fig. 2. (Color online) More refined theoretical photoionization spectra (top plot) of He atom from the 1s2p ^{1}P bound excited state to the ^{1}D continua and the corresponding variation of η_{tot} (bottom plot).

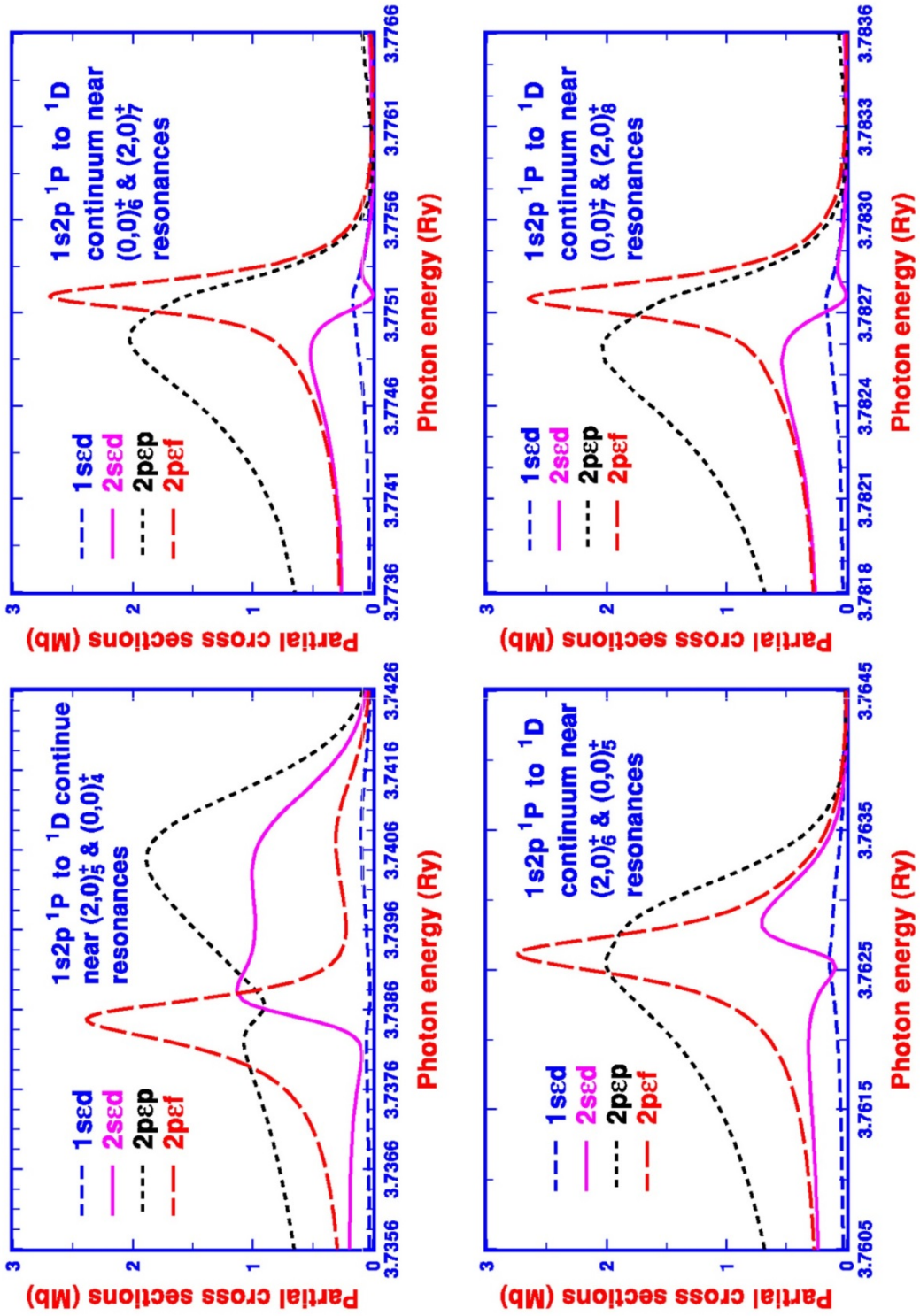

Fig. 3. (Color online) Partial photoionization cross sections for four pairs of closely spaced ^{1}D resonances.

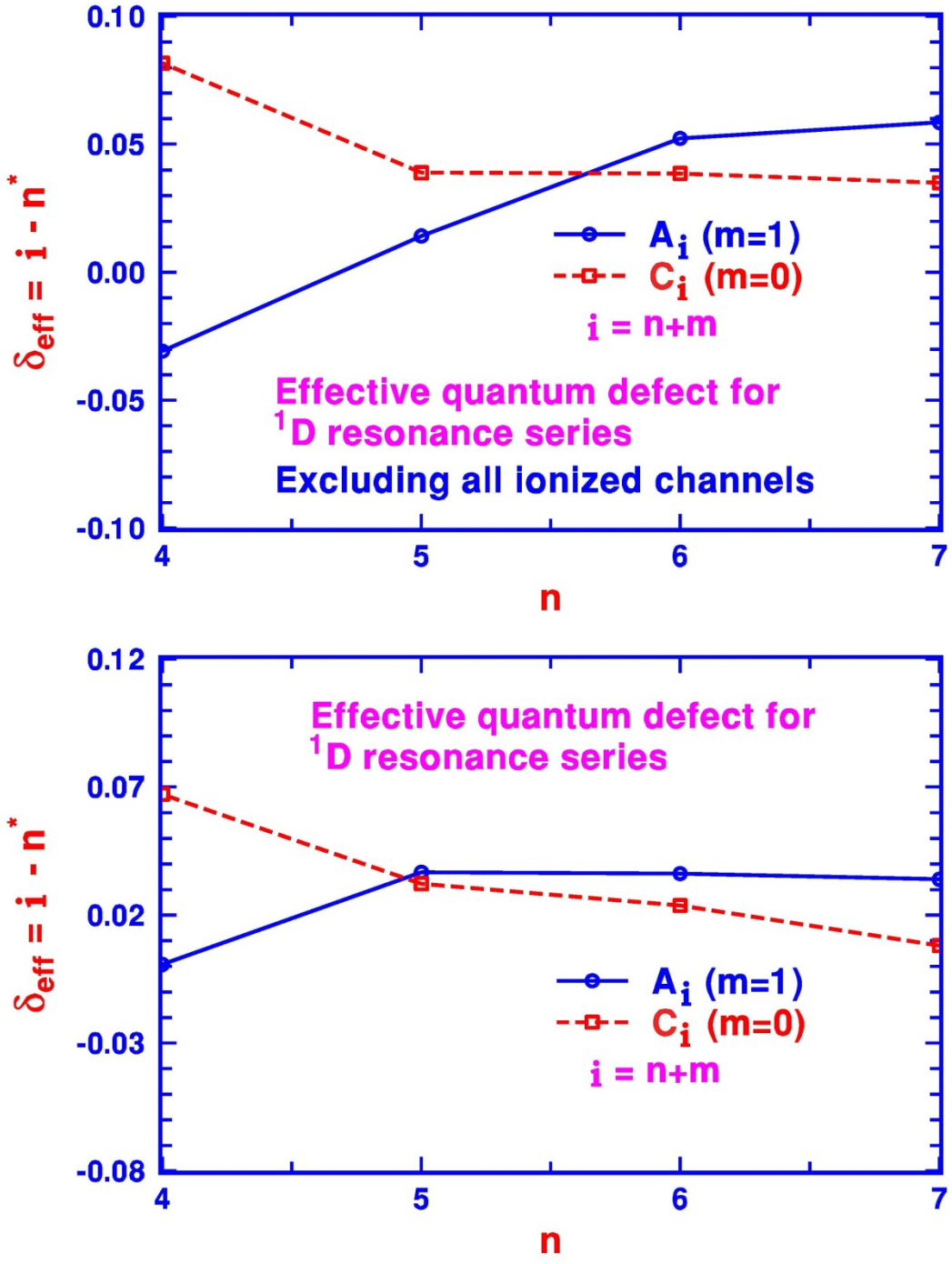

Fig. 4. (Color online) Variation of the theoretical effective quantum defects for two of the He ^{1}D resonance series A_i and C_i between the N=2 and N=3 thresholds.

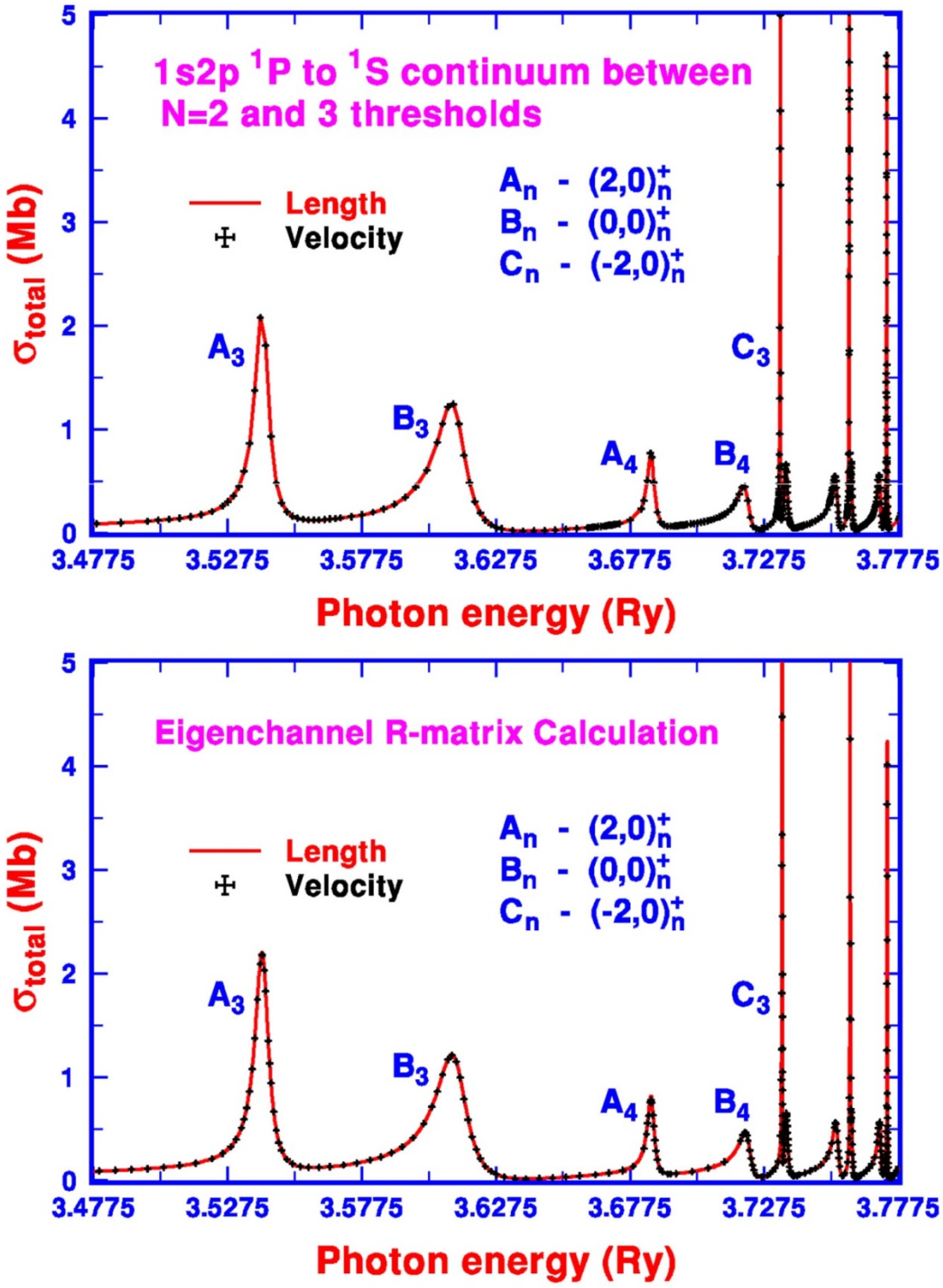

Fig. 5. (Color online) The theoretical photoionization spectra of He atom from the 1s2p ^{1}P bound excited state to the ^{1}S continua between N=2 and N=3 thresholds calculated with BSK method (top plot) and ECR method (bottom plot).

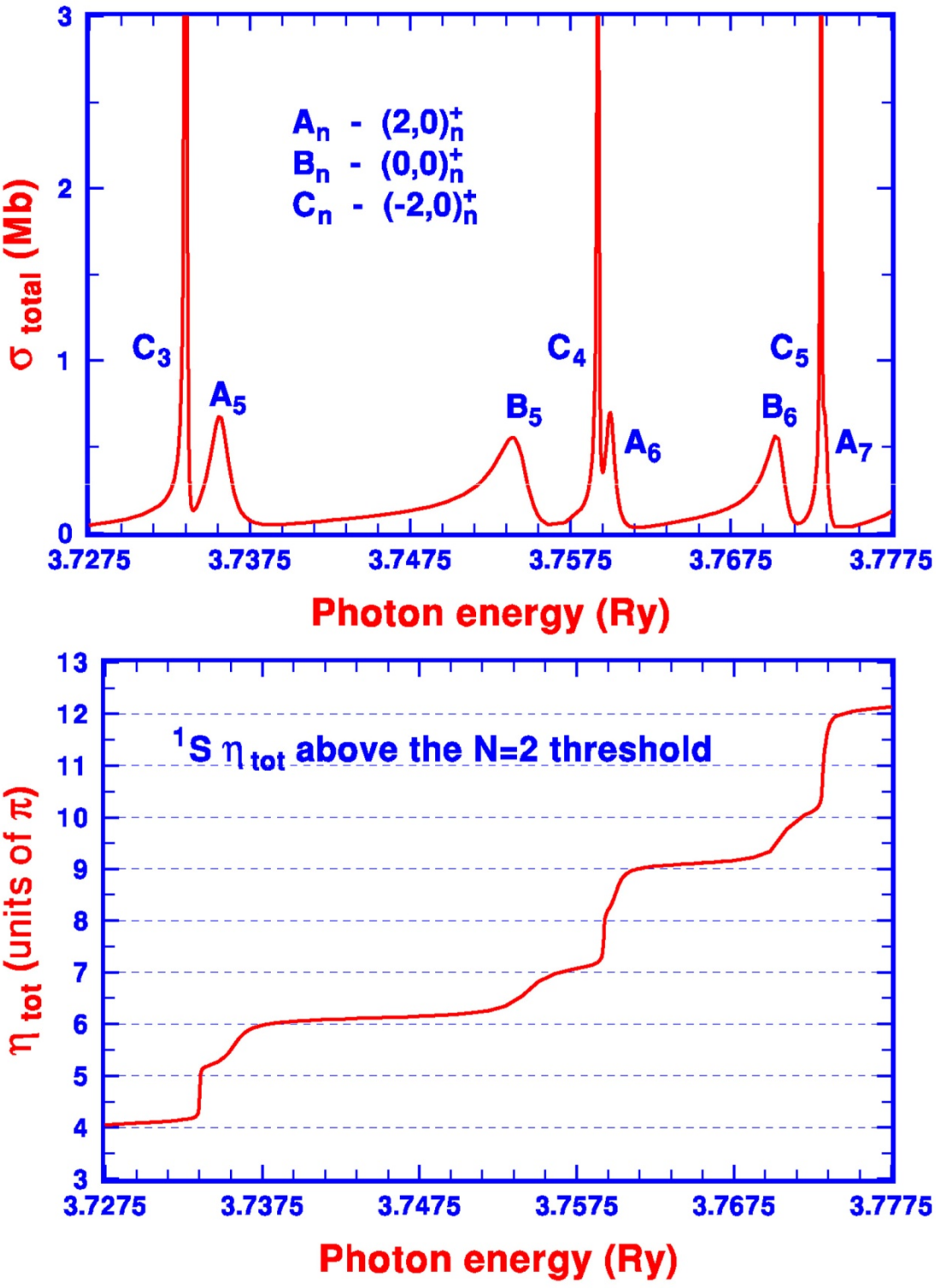

Fig. 6. (Color online) More refined theoretical photoionization spectra (top plot) of He atom from the 1s2p ^{1}P bound excited state to the ^{1}S continua and the corresponding variation of η_{tot} (bottom plot).

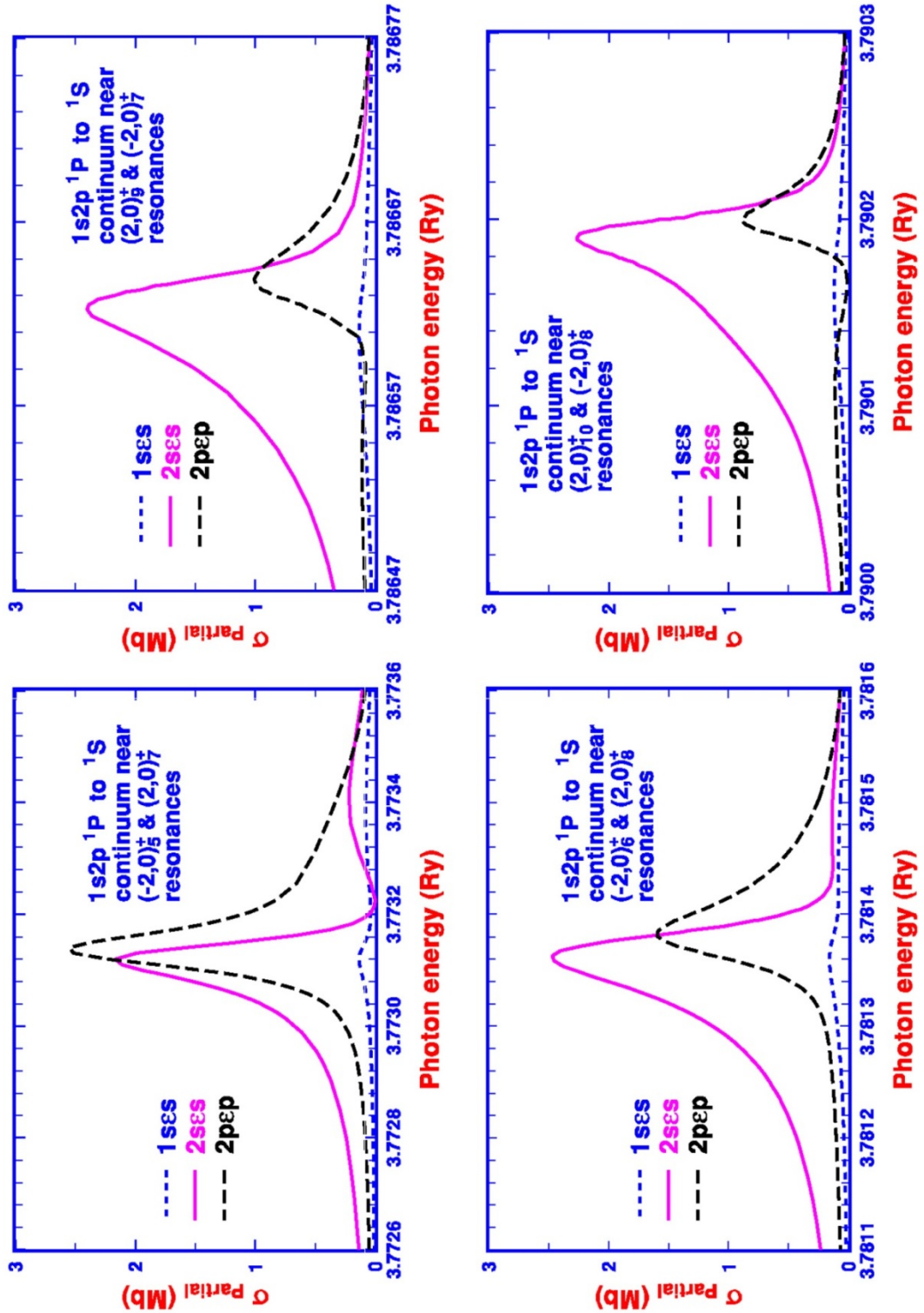

Fig. 7. (Color online) Partial photoionization cross sections for four pairs of closely spaced ^{1}S resonances.